Spectral properties of size-invariant shape transformation

Alhun Aydin*
Department of Physics, Harvard University, Cambridge, Massachusetts 02138, USA
and Department of Physics, Koç University, 34450 Sarıyer, Istanbul, Turkey

(Received 21 February 2023; accepted 21 April 2023; published 4 May 2023)

Size-invariant shape transformation is a technique of changing the shape of a domain while preserving its sizes under the Lebesgue measure. In quantum-confined systems, this transformation leads to so-called quantum shape effects in the physical properties of confined particles associated with the Dirichlet spectrum of the confining medium. Here we show that the geometric couplings between levels generated by the size-invariant shape transformations cause nonuniform scaling in the eigenspectra. In particular, the nonuniform level scaling, in the direction of increasing quantum shape effect, is characterized by two distinct spectral features: lowering of the first eigenvalue (ground-state reduction) and changing of the spectral gaps (energy level splitting or degeneracy formation depending on the symmetries). We explain the ground-state reduction by the increase in local breadth (i.e., parts of the domain becoming less confined) that is associated with the sphericity of these local portions of the domain. We accurately quantify the sphericity using two different measures: the radius of the inscribed n-sphere and the Hausdorff distance. Due to Rayleigh-Faber-Krahn inequality, the greater the sphericity, the lower the first eigenvalue. Then level splitting or degeneracy, depending on the symmetries of the initial configuration, becomes a direct consequence of size invariance dictating the eigenvalues to have the same asymptotic behavior due to Weyl law. Such level splittings may be interpreted as geometric analogs of Stark and Zeeman effects. Furthermore, we find that the ground-state reduction causes a quantum thermal avalanche which is the underlying reason for the peculiar effect of spontaneous transitions to lower entropy states in systems exhibiting the quantum shape effect. Unusual spectral characteristics of size-preserving transformations can assist in designing confinement geometries that could lead to classically inconceivable quantum thermal machines.

DOI: 10.1103/PhysRevE.107.054108

I. INTRODUCTION

Spectral geometry deals with the relationships between the spectrum of a differential operator and the geometry of the manifold on which it acts [1]. With the remarkable progress in nanoscience and nanotechnology in the past few decades, understanding the spectra of finite-size systems has become crucial for the geometric design of nanostructures with enhanced physical properties [2–4]. In quantum confined systems, the discrete energy spectra make the geometry dependence of the physical properties of materials prominent, which were negligible at macroscale [5–9]. The quantum size effect is perhaps the best known of the geometric effects appearing at nanoscale [10–13] and the importance of the energy quantization and few-level systems has led to the study of quantum heat machines highlighting the essence of this effect [14–22].

Recently, the size-invariant shape transformation (SIST) technique has been introduced to completely separate size and shape effects from each other [23]. By applying this technique to the domain where particles are confined, one can define control variables uniquely characterizing the shape of the domain. Then, for strongly confined systems, the quantum shape effect is defined as the characteristic changes in physical properties due to changes in the corresponding shape variable controlling the shape. SIST lies in the heart of quantum shape effects. Quantum shape effects can cause classically impossible thermodynamic behaviors, most notably allowing spontaneous thermodynamic transitions to lower entropy states [23]. Among many possible applications, it is demonstrated that they can be used to design novel thermodynamic cycles [23] and to harvest energy based on core-shell nanostructures [24]. In fermionic systems, the Fermi level can effectively be controlled by shape to utilize the oscillations in thermodynamic and transport properties caused by quantum confinement [25]. All of these quantum shape-dependent behaviors can be traced back to their roots in the eigenspectra of the confining media. Both to develop a deeper understanding of quantum shape effects and to explain the fundamental underlying reasons for their consequent phenomena, the examination of the eigenspectra under the SIST is needed.

In this paper, we start by exploring the properties of the Dirichlet spectrum of the Laplacian for confined geometries undergoing the SIST. We show that varying the shape of a domain by preserving its sizes amounts to creating a geometric coupling between otherwise independent levels, resulting in a nonuniform energy level scaling that is characterized by two distinct changes in the Dirichlet spectrum: (1) the decrease of the smallest eigenvalue, which we refer to as

*alhunaydin@fas.harvard.edu

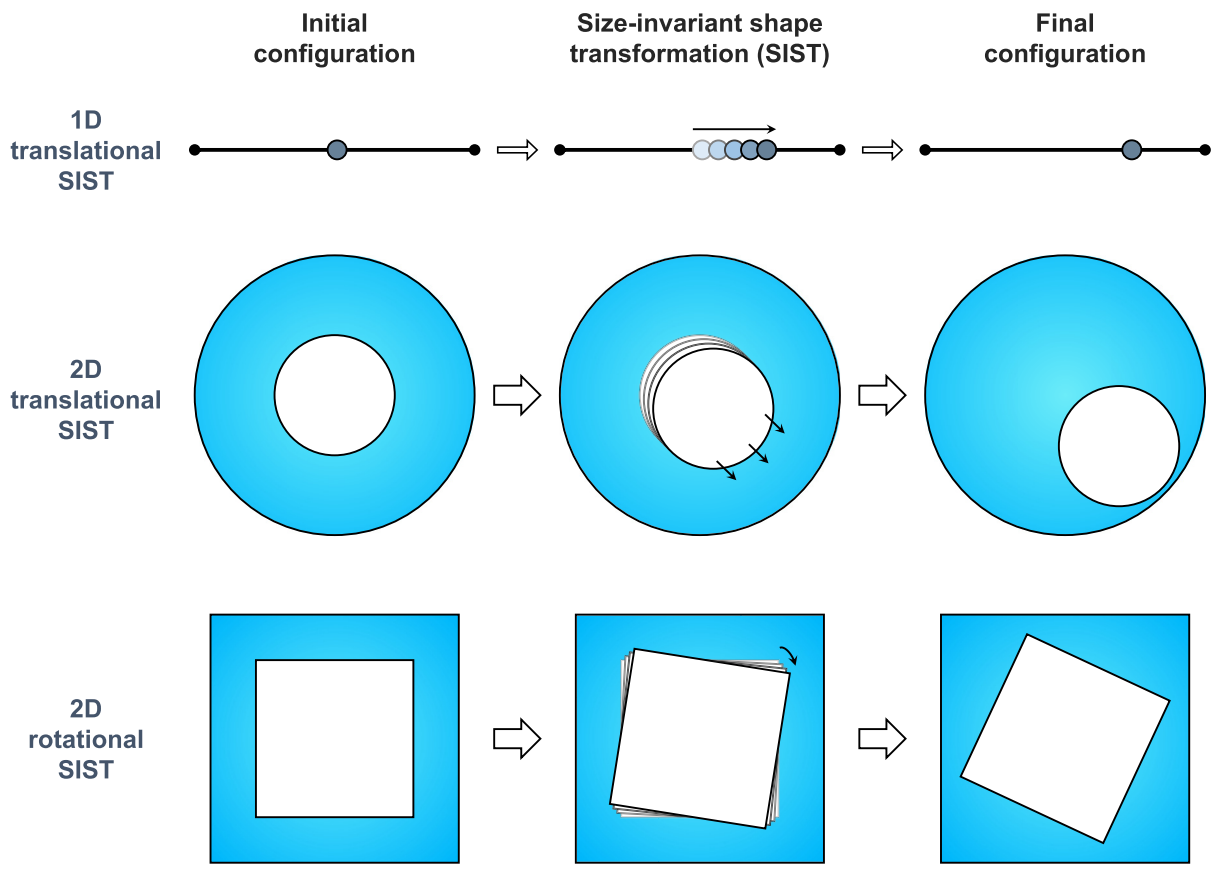

FIG. 1. Examples of SIST. The first and last columns show the initial and final configurations of the examined shapes, whereas the middle column shows the applied transformations. The first row shows the translation of an inner boundary inside a 1D domain. A 2D version of the same concept is shown in the middle row, represented by nested circles. Rotation of the inner domain is another transformation in 2D. Examples can be extended to higher dimensions without loss of generality. All transformations preserve the sizes under the Lebesgue measure while changing the shape of each domain.

the ground-state reduction, and (2) changes in gaps between eigenvalues due to degeneracy formation or level splitting, depending on the initial configuration spectra and the type of SIST applied. Moreover, we explain the underlying reasons for these changes. The first mechanism occurs as a result of the fact that the shape of the local regions inside the domain becomes similar to the shape of an n-dimensional sphere (n-sphere), which affects the spectra in a way that reduces the first eigenvalue, as a consequence of Rayleigh-Faber-Krahn inequality. Apart from being a direct measure of sphericity, the radius of the inscribed n-sphere serves also as a good measure of the ground-state reduction, which also helps to understand its underlying cause: the increase of local breadths. The second mechanism in turn arises from the requirement that the asymptotic behavior of the eigenvalues must be the same under the effect of ground-state reduction, as a consequence of the Weyl law. These two phenomena underlie the reason for the nonuniform level scaling and its counterintuitive thermodynamic consequences, such as the spontaneous and simultaneous decrease in free energy and entropy. In addition, we provide a physical understanding of such behaviors by proposing the existence of a quantum thermodynamic phenomenon, directly coming from our spectral analysis, which we call the quantum thermal avalanche. Our findings provide a fundamental understanding and explanation of the peculiarities observed in the thermodynamic properties of particles due to the quantum shape effect.

II. TRANSFORMING THE SHAPE WHILE PRESERVING THE SIZE

The size of a domain is characterized by geometric size parameters that are defined under Lebesgue measure as volume $\mathcal{V}$, surface area $\mathcal{A}$, peripheral length $\mathcal{P}$, and the number of vertices $\mathcal{N}_{\mathcal{V}}$ (i.e., discontinuities in boundaries such as corners or cusps). They represent the contributions to the sizes of a domain of different integer dimensions in descending order from three dimensions (3D) to 0D. There is a simple and continuous way of changing the shape of a domain without altering any of these size parameters. It is called isometric (or, more precisely, size-invariant) shape transformation, which is visualized in Fig. 1 for various carefully chosen domains. The procedure of SIST can be described as follows: Consider any type of fixed domain shape in any dimension and introduce an inner domain with a boundary into it. It can be a dot or a finite length in 1D or any other shape in higher dimensions that can be removed from the considered domain. Removing the inner domain leaves the remaining domain that we are interested in, e.g., denoted by blue regions in Fig. 1. Now one can apply translation or rotation to the inner domain that

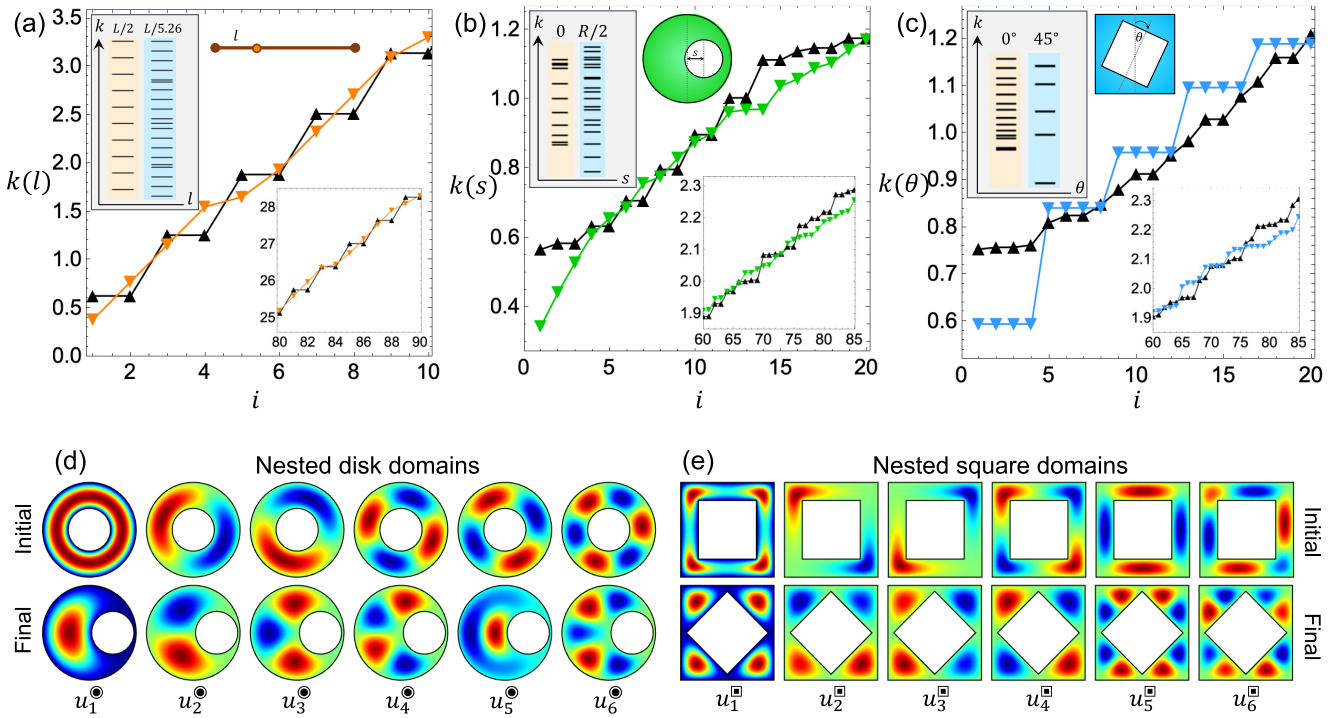

FIG. 2. Nonuniform level scaling in spectra under SISTs due to geometric level couplings. Eigenvalue k versus its number i plots for (a) a 1D domain with length L undergoing translational SIST, (b) nested 2D disks with outer disk radius R undergoing translational SIST, and (c) nested 2D squares undergoing rotational SIST. SISTs are characterized by the shape variables l, s, and θ, respectively, whose meanings are illustrated in the inset figures showing the domains. Geometric level couplings are created by the corresponding shape variables. Eigenspectra of the initial (final) configurations are given by the black (colored) up(down)-triangles. For easy comparison, the first 20 eigenvalues are also shown as level-line plots in the boxed inset figures. Values of the shape variables for initial and final configurations are typed on top of their respective level spectra. An arbitrary portion of the higher eigenvalue spectra is also given as inset figures on the bottom-right of each subfigure. (d) First six eigenfunctions of nested disk and (e) nested square domains. The top and bottom rows show initial and final configurations, respectively.

has been removed, which amounts to the continuous variation of the boundaries of the remaining domain. It is easy to notice that the sizes of the domain stay fixed under these transformations. In other words, SIST is not only volume preserving and area preserving but also a periphery-preserving and vertices-preserving operation. It preserves all geometric size variables together. We show only a few examples in Fig. 1, but actually this technique is quite general and can be applied to objects in any shape or dimension. It allows us to construct arbitrarily shaped domains where we can change the shape without altering any of the geometric size parameters.

III. NONUNIFORM LEVEL SCALING DUE TO GEOMETRIC LEVEL COUPLING

Consider the Dirichlet problem for the Laplacian on a domain Ω

$$\nabla^2 u + \lambda u = 0 \quad \text{on } \Omega, \quad u|_{\partial\Omega} = 0, \tag{1}$$

where λ and u are the Dirichlet eigenvalues and eigenfunctions and $\partial\Omega$ is the domain boundary. This eigenvalue problem is equivalent to finding the fundamental and overtones of a drum [26–29], modes of a waveguide [30–35], or a quantum billiard [36–38] or finding the energy levels of electrons confined in a box with shape Ω [39–41]. Thus, Eq. (1) is equivalent to the Helmholtz equation and time-independent Schrödinger equation, $\nabla^2 u + k^2 u = 0$, where k is the momentum eigenvalue. Henceforward, we will use momentum eigenvalues, k's, to examine the spectra under SISTs because of their immediate connection to the thermodynamic results given in Sec. VII.

Now think of a drumhead with an elastic membrane in one of the shapes of 2D domains shown in Fig. 1. By applying SIST, we can prepare another drumhead and compare how they sound. Although the surface area $\mathcal{A}$ as well as all other size variables (such as the lower-dimensional ones, i.e., $\mathcal{P}$ and $\mathcal{N}_\mathcal{V}$) of both drumheads are exactly equal to each other, spectra of the membranes will be different [23]. In other words, the domains constructed by SIST are not isospectral. They will sound different as the normal modes of the membranes would be different. In fact, under SIST, the most distinct one of all modes will be the fundamental mode of the membranes, which we will explore in next section.

We consider three domains given in Fig. 1 and calculate each of their Dirichlet eigenvalues and eigenfunctions by numerically solving Eq. (1). We investigate the variations of their eigenspectra under their respective SISTs in Fig. 2. The first example we look at is a 1D domain with an inner boundary and the translation of this inner boundary to either left or right. One can think of this as a particle in a box separated

by a movable but impenetrable partition. This is actually the simplest case of a SIST which is comprehensively examined in Ref. [42]. The distance of the inner boundary (movable partition) from the outer one (the left boundary is chosen as a reference) is denoted by l, which comes out as the shape control variable of this 1D translational SIST, see Fig. 2(a). The partition could be chosen to have any finite thickness, and here we choose it as zero thickness. For this simple system, eigenspectrum can be obtained analytically as the union of the eigenvalue spectra of left and right compartments,

$$k_i(L,l) = k_i'(l) \cup k_i'(L,l) = \left\{\frac{\pi i'}{l}\right\} \bigcup \left\{\frac{\pi i'}{L-l}\right\}, \quad (2)$$

where $i, i' = 1, 2, 3, \ldots$, eigenstate numbers. We plot the first 10 eigenvalues in Fig. 2(a), the eigenvalue number being denoted by i. The spectrum of the initial configuration (the inner boundary is chosen at the center, $l = L/2$) is given by the black up-triangles and of the final configuration (the inner boundary is at a close distance to the outer boundary, $l = L/5.26$) by the orange down-triangles. The values are presented as joined data for convenience. We plot the first 20 eigenvalues also as a level-line plot in the boxed inset figure to make easier comparisons of spectral modifications. An arbitrarily chosen higher portion of the eigenvalue spectrum is plotted as another inset figure. A similar convention is followed for the other shapes that we consider. In Fig. 2(b) we examine the spectrum of the second domain composed of nested disks (the smaller one is removed from the larger one) undergoing 2D translational SIST with a shape variable s being the distance of the inner disk's center from the center of the outer disk. The initial configuration is chosen as concentric ($s = 0$) and in the final configuration inner disk is slid to the right to be centered at $s = R/2$, where R is the radius of the outer disk. As the third example, the spectra of nested concentric squares undergoing 2D rotational SIST are shown in Fig. 2(c). Here SIST is characterized by the rotation angle of the inner square, θ, initially at $\theta = 0^\circ$ and finally at $\theta = 45^\circ$.

As is seen in Fig. 2, all types of SISTs cause nonuniform scaling of the eigenspectra. This is a peculiar behavior coming from the creation of a geometric coupling between the levels due to SISTs. Normally, eigenstates are influenced uniformly and linearly by the changes affecting the spectrum. For example, changing the length of a domain in any direction causes a uniform or linear scaling of the levels in that particular direction (e.g., doubling the length reduces the energy to a quarter in a particle in a box), or opening an external field shifts the spectrum as a whole, again corresponding to a uniform or linear scaling. In fact, all conventional thermodynamic control variables like volume, temperature, external field parameters, and so on, cause linear transformations (uniform scalings or shifts) on the eigenspectra. On the other hand, the property of size invariance induces a geometric coupling between otherwise-independent levels. This can be most easily seen in Eq. (2) where the spectrum of the domain is composed of the union of the spectra of two spatially independent but geometrically coupled domains. The geometric coupling parameter is the position of the partition, l. Due to this additive coupling, levels are no longer independent and changes in l nonuniformly affect the spectrum. The same phenomenon occurs in the other two types of SISTs. However, shape variables of the domains in higher dimensions have complicated functions of the eigenvalues and, in general, it is not possible to obtain the spectrum analytically to examine the exact functional forms of these geometric couplings. Nevertheless, even examining them numerically provides important insights into the nature of the phenomenon of nonuniform level scaling.

While nonuniform level scaling provides a global perspective on the eigenspectra, here we go beyond and look further in detail to find out the underlying reasons for these types of modifications in the eigenspectra due to SISTs. There are two notable common modifications. The first and the most noticeable one is the lowering of the first eigenvalue, as it can be directly seen in all three cases that we consider in Fig. 2. The second is the breaking of degeneracies or equivalently the splitting of levels. Both have important consequences on the physical properties of particles confined in such systems. In the next section, we examine the underlying reason for the lowering of the first eigenvalue.

IV. GROUND-STATE REDUCTION DUE TO SPHERICITY

Before explaining the lowering of the first eigenvalue under SIST, it is tempting to question the direction of the transformation. After all, we could reverse the initial and final configurations, which would still be considered as a SIST, but the first eigenvalue would have been increased in such a case. Essentially, there is a physical reason for choosing the direction of the transformation in the specified way. We choose the initial configurations in such a way that it maximizes the Helmholtz free energy of the noninteracting particles confined inside the domains at a constant temperature. As such, when systems are perturbed from their respective initial configurations, they spontaneously transition into their respective final configurations under a quasistatic process. Since all thermodynamic-state variables stay constant under this transition except the corresponding shape variable, the changes in free energy are solely due to the shape transformation. Quantum shape effects also maximize when going from initial to final configurations, which is another reason we choose the direction of the transformation in the prescribed way.

In quantum-confined nanostructures, the sizes are comparable to the thermal de Broglie wavelength of particles so that only a few states can be thermally excited. Under such conditions, the influence of SIST on the physical properties of spatially confined particles is called quantum shape effect [23]. Quantum shape effects can be quantified analytically by invoking the quantum boundary layer concept [43–45] and defining an effective n-volume considering the overlaps of quantum boundary layers [23,46]. See the Appendix for details. Both the quantum boundary layers and their overlaps are temperature-dependent quantities which bring both shape and additional temperature dependence to thermodynamic properties. Overlaps of quantum boundary layers occur when inner and outer boundaries come very close to each other. They increase the effectively available domain for particles to occupy. As long as the inner boundaries are at a far-enough distance from the outer ones, overlaps will not be appreciable and quantum shape effects vanish. The more the overlap, the larger the quantum shape effects. Hence, we choose the direction of

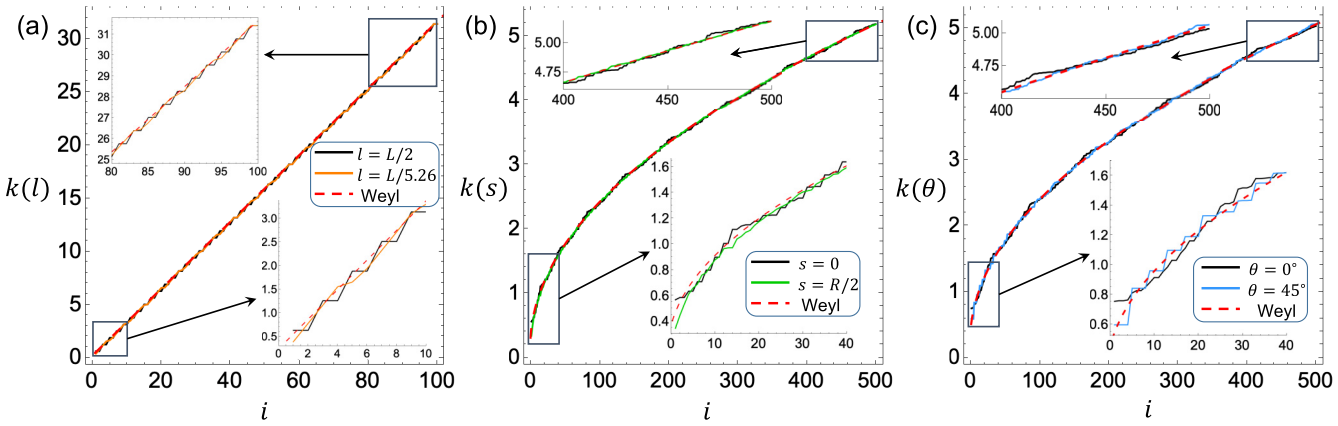

FIG. 3. Accuracy of Weyl law in predicting the asymptotic as well as average behaviors of eigenspectra of size-invariant domains having different shapes. Weyl law, however, fails to predict any shape difference. Eigenvalue spectra of (a) 1D domain under translational SIST, (b) 2D domain composed of nested disks under translational SIST, and (c) 2D domain composed of nested squares under rotational SIST. Initial and final configurations are represented by black and colored curves, respectively. Weyl curves are found simply by solving Eq. (4) for k. Inset figures show the zoomed versions of the selected portions of spectra.

SIST in the way that quantum shape effects increase. Final configurations have more shape dependence than the initial ones. Thus, the reduction of the ground state happens to be a characteristic property of the quantum shape effect.

To understand how quantum shape effects lead to a persistent lowering of the ground states, we start by noticing the immediate connection between the eigenspectrum and the geometric size parameters. This connection is quantified by Weyl law describing the asymptotic behavior of the Dirichlet eigenvalues of the Laplacian in terms of the geometric size parameters under the Lebesgue measure [2,47,48]. The asymptotic expression of the number of eigenvalues less than k for the Helmholtz equation can be written in its general, D-dimensional, closed form [46] as

$$W_D(k) = \sum_{n=0}^{D} \left(-\frac{1}{4}\right)^{D-n} \left(\frac{k}{2\sqrt{\pi}}\right)^{n} \frac{\mathcal{V}_n}{\Gamma[n/2+1]}, \tag{3}$$

where $\mathcal{V}_n$ is the n-dimensional volume under the Lebesgue measure ($\mathcal{V}_3 \to \mathcal{V}$, $\mathcal{V}_2 \to \mathcal{A}$, $\mathcal{V}_1 \to \mathcal{P}$, $\mathcal{V}_0 \to \mathcal{N}_\mathcal{V}$). Since we are dealing with 1D and 2D domains, let us write their explicit Weyl expressions (we also write 3D one for completeness) respectively as

$$W_1(k) = \frac{\mathcal{P}}{\pi}k - \frac{\mathcal{N}_\mathcal{V}}{4}, \tag{4a}$$

$$W_2(k) = \frac{\mathcal{A}}{4\pi}k^2 - \frac{\mathcal{P}}{4\pi}k + \frac{\mathcal{N}_\mathcal{V}}{16}, \tag{4b}$$

$$W_3(k) = \frac{\mathcal{V}}{6\pi^2}k^3 - \frac{\mathcal{A}}{16\pi}k^2 + \frac{\mathcal{P}}{16\pi}k - \frac{\mathcal{N}_\mathcal{V}}{64}. \tag{4c}$$

There is also a variant of Eq. (3) with an additional term related to the number of holes inside the domain [26,29]. The number of holes term gives zero contribution for a single hole and it is valid for domains with smooth boundaries, which is not satisfied by all the domains that we considered here. Hence, we omit the term related to the number of holes.

In Fig. 3, we compare the actual eigenspectra of initial and final configurations (i.e., the ones that are the most radically different) under SIST with the predictions of Weyl law for different domains. Weyl law quite accurately predicts the behaviors of eigenvalues even for low-lying ones by passing around their averages [49]. It is also appropriate to mention here that the fact that Weyl law can successfully produce all the lower-dimensional quantum-size-effect corrections [49,50] relies on its remarkable success in predicting the behaviors of eigenvalues. This makes it a reliable tool to analytically study quantum size effects in confined systems via, for example, Weyl density of states [35,42,49,50].

Dirichlet eigenvalues and eigenfunctions are directly determined by the shape of the domain. Besides the global size and shape of domains, local shape information is also embedded in the eigenspectra [51–53]. In fact, for concave or hollow domains (like the ones we consider here), the shapes of the local parts of the domain could be even more decisive in determining the characteristic spectra [23]. All geometric size parameters remain unchanged under SIST, which means Weyl law gives exactly the same values and cannot distinguish the shape difference, see Fig. 3. Since Weyl law is basically an asymptotic theorem, it cannot predict the changes due to SIST. Nevertheless, it is possible to extract some useful information by studying the form of the Weyl expressions. For instance, Weyl's law states that the bulk terms ($\mathcal{P}$ in 1D and $\mathcal{A}$ in 2D) have the largest effect on the eigenspectrum. Although geometric size variables are preserved globally under SIST, arbitrarily selected parts of the domains can have different sizes locally. Therefore, we could get insights into the behavior of the first eigenvalue by investigating the local confinements, whose information is embedded in the eigenvalues and eigenfunctions. See, for instance, Figs. 2(d) and 2(e), where we plot the first six eigenfunctions for the initial and final configurations of nested disk and square domains, respectively. Now imagine cutting the nested disk domain vertically into two halves and consider the left half during SIST [see how the first eigenfunction varies in Fig. 2(d)]. We can notice that the first eigenfunction experiences as if the domain is larger in the final configuration compared to

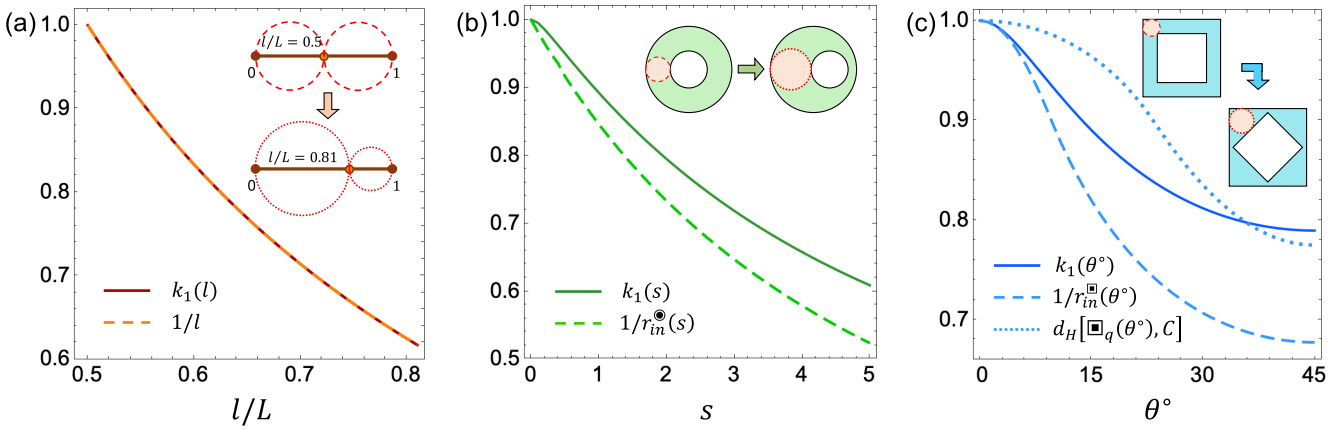

FIG. 4. Decrease of the ground state with respect to shape variables can be understood by the increase of breadth and sphericity of the local parts of the domain. All values are normalized by the values of their respective initial configurations. Solid curves represent the variation of the first eigenvalue with the corresponding shape variable of (a) a 1D domain with an internal boundary, (b) a 2D domain of nested disks, and (c) a 2D domain of nested squares. Local breadth is measured by the radii of inscribed circles, which are shown by dashed curves. Ground-state reduction is associated with the enlargement of the inscribed circles. As local breadths and first eigenvalues are inversely proportional, inverses of the local breadth measures are plotted. The dotted function represents the Hausdorff distance measuring the sphericity. The shorter the Hausdorff distance, the more spherelike the object.

the initial one. Even though the area stays fixed *globally*, translating the inner disk to the right leaves more area *locally* in the left part of the domain. The ground-state eigenfunction cannot fit into the narrow parts of the final configuration and experiences a larger domain overall, compared to the initial configuration. Then, from the inverse proportionality of size variables with eigenvalues, we expect the final configuration to have a lower first eigenvalue.

A similar argument can be made also for the 1D domain as well as the 2D nested square domain. In the 1D case, there is a larger length for the ground-state eigenfunction to occupy when the inner boundary is closer to the outer boundaries compared to the initial configuration where the boundary is at the center. While the confinement of one part causes the deconfinement of the other during the movement of the partition, the overall effect is actually asymmetric because of the decay of occupation probabilities in the smaller part. Hence, when the boundaries come very close to each other, they become almost indistinguishable (i.e., acting as if it is a single boundary) for the confined particles, which amounts to the local breadth of the larger part.

Note that in the case of the nested square domain, the geometric size variables are the same even for each quadrant under SIST (quadrant is defined considering nested squares being concentric at the origin). Still, a triangle-like shape (quadrant at $\theta = 45^\circ$) is perceived as less confined for the ground-state eigenfunction compared to a bent tube shape (quadrant at $\theta = 0^\circ$).

To refer to these less confined regions of a domain, we will use the word "breadth", whose third meaning in dictionary.com [54] stated as "freedom from narrowness or restraint" describes quite well what we would like to verbalize. We argue that there is a direct correspondence between the lowering of the first Dirichlet eigenvalue and the increasing of the local breadths of our domains. To quantify this, we propose the radius of the inscribed n-sphere (circle in 2D) as a measure. An inscribed circle is the largest circle that can fit into a 2D domain. Then, we conjecture that the larger the radius of the inscribed circle that we can fit into the domain, the lower the first eigenvalue:

$$k_1 \propto \frac{1}{r_{\text{in}}^{\Omega}}, \tag{5}$$

where k_1 is the nonzero first eigenvalue and r_{in}^{Ω} is the radius of an inscribed circle of a domain Ω.

The connection between the inverse radii of the inscribed circles of domains and their lowest Dirichlet eigenvalues is shown in Fig. 4. There we show the variation of the first eigenvalue (solid curves) with corresponding shape parameters and the predictions of our local breadth measure (dashed curves). For the convenience of comparison, all curves are normalized to their initial values at their initial configurations. In the 1D domain, the local breadth can directly be quantified by the inverse distance of the inner boundary to the outer one ($1/l$), which is equivalent to the inverse diameter of the inscribed circle in the 1D case, Fig. 4(a). While the local breadth measure exactly matches with the behavior of the first eigenvalue in 1D, this is trivial because the eigenvalue spectrum is in fact already inversely proportional to the domain lengths, i.e., the first eigenvalue is $k_1(L, l) = \min(\frac{\pi}{l}, \frac{\pi}{L-l})$.

A two-dimensional analog of the increase in local breadth due to translation can be seen in Fig. 4(b). In this case, the inner disk shifts to the right and increases local breadth in the left portion of the domain. The inverse of the increase of the inscribed circle radius matches quite well with the decrease of the first eigenvalue. The case of 2D rotational SIST is shown in Fig. 4(c), where again the inscribed circle method captures the functional behavior of the first eigenvalue under shape variation. As is seen, the inscribed n-sphere method provides a good measure for capturing the inverse proportionality between the local breadths and the first Dirichlet eigenvalues.

A quite related concept here is the isoperimetric inequality which states that among all shapes the circle (or n-sphere in general) has the largest surface area for fixed peripheral lengths [55]. The immediate connection of this fact to the eigenspectrum is provided by Rayleigh-Faber-Krahn inequality, which states that among all shapes having equal area, the circle has the lowest first Dirichlet eigenvalue [51,55–57]. This suggests that between shapes of equal sizes, the one that resembles most to a circle should have the smallest first eigenvalue. In fact, in the literature, inscribed circle has already been used as one of the methods that are proposed to distinguish shapes from each other and quantify their resemblance [58,59].

Another measure for local breadths is the sphericity of a domain. Sphericity is defined as a measure of how spherical (circular in 2D) an object is. There are several measures of sphericity in the literature and one of them is in fact the ratio of the radii of circumscribed and inscribed circles [59,60]. This is exactly the same as our local breadth measure since the radii of circumscribed circles do not change under SIST for any domain shape. In fact, isoperimetric inequality already implies that the local breadth and sphericity carry the very same meaning. The fact that a circle has the largest area of all isoperimetric objects makes it the best choice to describe the breadth of a domain that quantifies the largeness of local areas.

Hausdorff distance is one of the reliable measures for the similarity of two domains [61–64], which is also used in symmetrization methods [65]. Hausdorff distance representing the similarity of the shape of a domain Ω to the shape of a disk C is defined [61] as

$$d_H(\Omega, C) = \max\left[\sup_{\omega\in\Omega}\inf_{c\in C} d(\omega, c), \sup_{c\in C}\inf_{\omega\in\Omega} d(\omega, c)\right], \quad (6)$$

where $d(\omega, c)$ is the distance between the point ω in the region Ω and point c in the region C. It gives the best results for nonhollow domains, so we can use it to quantify the similarity of the quadrant in nested square domains to a circle. Consider dividing the nested square domain into its quadrants by taking the origin at the center of the squares. Each quadrant is identical to others as they are symmetric about the axes at all rotational configurations. At the initial configuration of $\theta = 0^\circ$ it starts from a bent tube shape and transitions into an obtuse triangle shape in the final configuration of $\theta = 45^\circ$. One can intuitively say that the final configuration looks more like a circle. When we measure the Hausdorff distance of the formed shapes to a disk, we find this is indeed the case. The shorter the Hausdorff distance, the more spherical the object. Since sphericity is related to the first eigenvalue via Rayleigh-Faber-Krahn inequality, we conjecture that Hausdorff distance to a disk should also give an estimate of the behavior of the first eigenvalue such that

$$k_1 \propto d_H(\Omega_p, C), \quad (7)$$

where Ω_p with the subscript p denotes a chosen part (one quadrant in this case) of the domain Ω. In Fig. 4(c), the variation of Hausdorff distance with the rotation angle is plotted by the dotted curve, which accurately describes the behavior of the first eigenvalue. Note that both the Hausdorff and incircle methods are proposed just to understand the ground-state reduction qualitatively. One should not expect a perfect quantitative match, as the actual behaviors of spectra are determined by the exact domain boundaries. However, we demonstrate that ground-state reduction is a consequence of the increased breadth and sphericity of the local parts of the domain, which appears as one of the characteristic properties of SIST.

V. LEVEL SPLITTING AND DEGENERACY DUE TO SIZE-INVARIANCE

The other characteristic change in the spectra of domains under SIST is the changes in spectral gaps. Level-line figures are shown in the insets of Figs. 2(a)–2(c). While the ground-state reduction was a common characteristic of any SIST, changes in spectral gaps are different for translational and rotational SISTs. In the case of translational SISTs, the initial configurations are the most symmetric ones. As can be seen from Figs. 2(a) and 2(b), degeneracies are prevalent at the initial configurations, but they vanish under translational SISTs, which breaks the symmetry inside the domain and cause level splitting. In such domains, the breaking of degeneracy and the occurrence of level splitting as a follow-up can be understood by the breaking of translational symmetry. On the other hand, under rotational SIST an opposite behavior occurs. More degeneracies are formed when the nested square domain undergoes rotational SIST, see Fig. 2(c). Essentially, this is intimately related to the characteristic shape of the domains; however, the main difference compared to the translational case is that rotational SIST preserves the axial symmetries of the initial configuration. Both initial and final configurations incorporate degeneracies for nested square domains. These degeneracies are visualized in eigenfunctions which can be seen in Fig. 2(e). The biggest difference is that there are four almost distinct chambers forming in each quadrant of the final configuration. Since the apex length (closest point of inner and outer boundaries) is chosen to be very narrow, low-lying eigenfunctions could not see other chambers and nest themselves into almost distinct chambers, promoting the four-fold degeneracy. In the initial configuration, on the other hand, the apex length (basically corresponds to the tube width) is large enough for low-lying eigenfunctions to fit, which creates less degeneracy compared to the final configuration. That is why eigenvalues are closer to each other at $\theta = 0^\circ$ and distant at $\theta = 45^\circ$ configurations. The level splittings we examine here are of geometric origin and can be thought of as geometric analogs of the Stark and Zeeman effects resulting from the presence of electric and magnetic fields.

We can quantify the changes in the spectral gaps by studying the level statistics. In Fig. 5, we plot the variation of the averaged differences between successive eigenvalues by removing degeneracies. Black and colored curves represent the initial and final configurations respectively. Mean spacing is defined by

$$\langle \Delta k \rangle_N = \sum_{i=1}^{N} \frac{k'_{i+1} - k'_i}{N}, \quad (8)$$

where prime superscripts denote the nondegenerate eigenvalues and N is the total number of eigenvalues that are

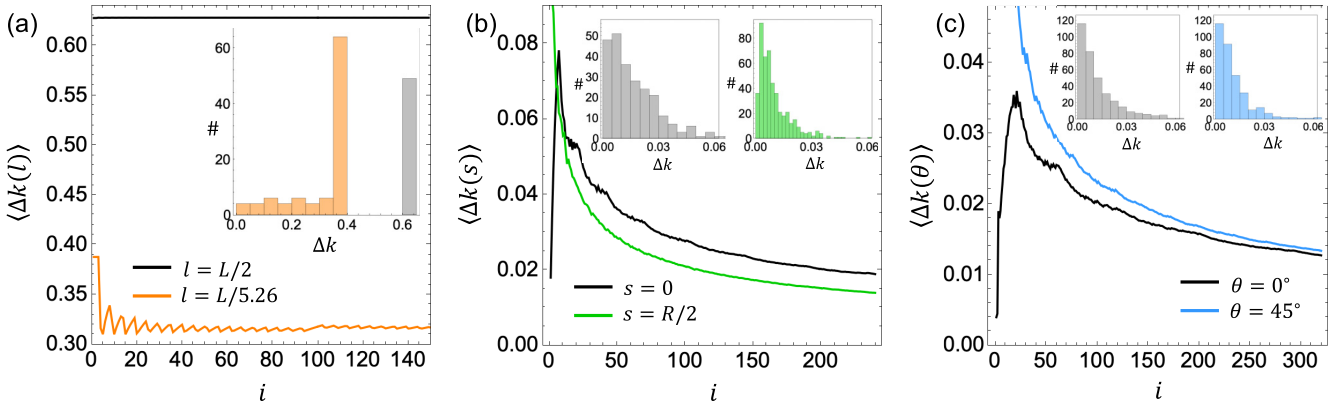

FIG. 5. Mean level spacings. Variation of the average differences (without degeneracies) between the levels (eigenvalues) with increasing level number i for (a) 1D domain, (b) 2D nested disks, and (c) 2D nested squares. Black and colored curves represent the initial and final configurations, respectively. Inset figures show the histogram of the level differences. Gray and colored histograms represent the initial and final configurations respectively.

considered. The degeneracies are removed in order to prevent them from improperly lowering the average values, as we are investigating specifically the gaps in this case. As we expected, for translational SISTs spectral gaps are larger in the initial configurations compared to the final ones, see Figs. 5(a) and 5(b) where black curves stay on top of the colored ones. On the other hand, the behavior is reversed and the black curve stays consistently below the blue curve in Fig. 5(c) showing that spectral gaps are larger in the final configuration compared to the initial one in rotational SIST. This is also pretty clear in Fig. 2(c).

We also plot histograms of nondegenerate level spacings as inset figures in Fig. 5. In the 1D case, spacing distributions are too wide apart to assign any statistical behavior. The initial configuration has a constant level spacing and the final configuration has a few spacing values, Fig. 5(a). In the nested disk case, when the system is perturbed from the initial configuration, the nearest-neighbor level spacings transition to be of Wigner-Dyson type, suggesting a chaotic behavior; see the green histogram in Fig. 5(b). In the nested square case, the level spacings unambiguously exhibit Poisson-type statistics, suggesting a regular behavior [66].

There is an immediate connection between the ground-state reduction and the behaviors of the spectral gaps. When a domain undergoes a SIST, the first eigenvalue decreases. However, as a result of the size-invariance condition, the domain also has to keep the same asymptotic behavior in accordance with the Weyl law. The only way to preserve the asymptotic behavior is to compensate for the ground-state reduction by opening spectral gaps in the excited states. This is clearly observed in Fig. 2(c) and it occurs also to some extent in nested disk domains as near-ground-state energy spacings could increase [e.g., the low-lying eigenvalue behavior in Fig. 5(b)]. It eventually leads to a behavior where both eigenspectra fluctuate around their Weyl asymptote. Since low-lying states are prominent in determining the physical properties of confined systems, the compensation of the ground-state reduction by the gap openings serves as an important characteristic of the spectra of systems exhibiting the quantum shape effect.

VI. WEAKLY SIZE-INVARIANT ANISOMETRY TRANSFORMATION

Before going into the physical consequences of the spectral changes due to SIST, we will also explore a subordinate effect of it. Rather than keeping all of the size parameters constant, one can consider keeping the bulk parameter (area in 2D) fixed and changing the anisometry of the domain. Take, for instance, a square domain and turn it into a rectangle by changing the side lengths in a way to keeps the area fixed. Although such a transformation is area preserving, it cannot preserve the periphery at the same time. We can call such a transformation a weakly size-invariant anisometry transformation. Here the term "weakly" indicates that it is not fully size invariant but invariant with respect to only some of the geometric size parameters.

Nevertheless, because of the area-preserving nature of the system, nonuniform level scaling in the eigenspectra for such weakly size-invariant anisometry transformations has already been observed [17,18,67,68]. As we argue here, such behaviors originate from the increased local breadth and obedience to the Weyl law. The sphericity of the square is higher compared to a rectangle with the same area, making the square configuration have the lowest eigenvalue of all other anisometric rectangles. Also, weak size invariance via area-preserving transformation causes the splitting of the levels. Under any type of size-invariant transformation, the geometric information of the perpendicular directions is no longer independent. The condition of preserving sizes induces a geometric coupling between the initial and final configurations of the transformed geometry. In this weakly size-invariant anisometric transformation, a multiplicative coupling is created between the sizes of two orthogonal directions, e.g., the initial configuration is a square with the side length of a and the final configuration is a rectangle with side lengths of a^2/b and b. The eigenvalue spectrum of such a system becomes

$$k_{i_1,i_2}(a,b) = \sqrt{\left(\frac{\pi i_1}{a^2/b}\right)^2 + \left(\frac{\pi i_2}{b}\right)^2}, \tag{9}$$

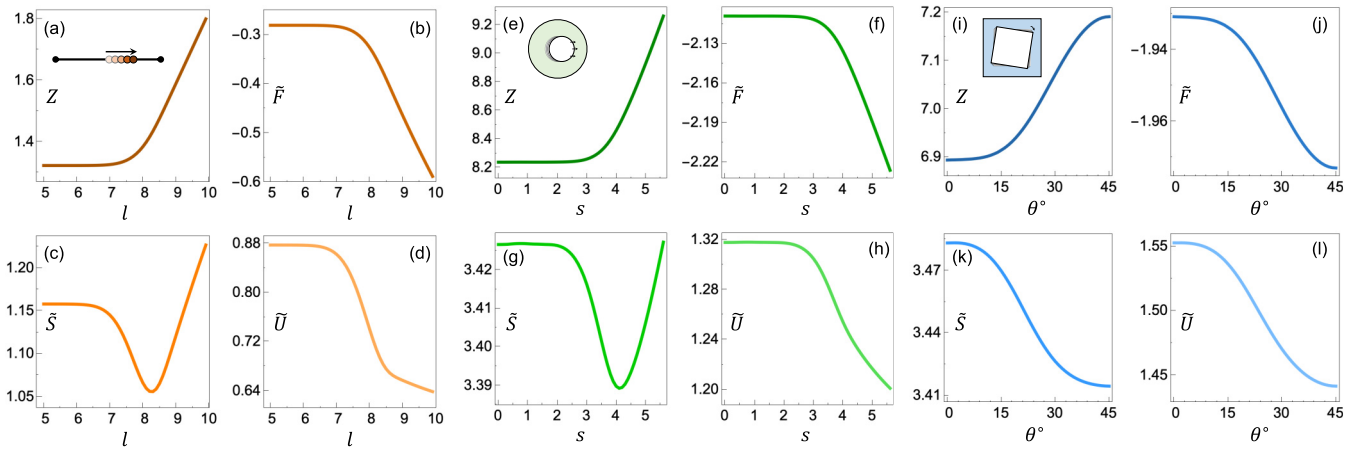

FIG. 6. Variation of thermodynamic properties with the corresponding shape variables. Curves with shades of red, green, and blue represent a 1D domain with a moving partition, a 2D nested domain with translating disk, and a 2D nested domain with a rotating square shown in inset, respectively. Thermodynamic properties are shown from darker to lighter shades of colors as a partition function, free energy, entropy, and internal energy, where the last three are normalized (to k_BT and entropy to k_B).

where $i_1, i_2 = 1, 2, 3, \ldots$ are the eigenstate numbers of two orthogonal directions. Here b serves as the coupling variable mediating the geometric coupling between two orthogonal directions. When $a = b$, the square configuration is recovered. Hence, the variations with respect to the variable b induce nonuniform scaling in the spectra. One drawback of this type of anisometry transformations is it is not quite easy to see how they can be achieved continuously under a quasistatic process. The continuous nature of the SIST processes makes them easier to physically realize. We do not go into the details of weakly size-invariant anisometry transformation to keep the focus on the full size invariance in this work.

VII. PECULIAR THERMODYNAMIC BEHAVIORS: ENTROPY ANOMALIES

In this section, we discuss a physical example where these spectral modifications manifest themselves causing some unexpected physical behaviors. Consider a quantum particle confined in a box at thermal equilibrium at a temperature T with a heat bath. The wave nature of the particle becomes significant when the boundaries of the domain are close enough to each other so that the sizes are in the order of the thermal de Broglie wavelength of the particle. One cannot consider it as a point particle and continuous spectrum approximation become invalid. Hence, there are deviations from the ideal gas behavior due to quantum size and shape effects [3,69,70]. Under quantum shape effects, in particular, thermodynamic-state functions exhibit peculiar behaviors never seen before in the classical thermodynamics of gases [23–25,46,71].

The canonical partition function of a particle confined in a domain is written as

$$Z = \sum_i \exp\left(-\frac{E_i}{k_BT}\right), \tag{10}$$

where k_B is Boltzmann constant, T is temperature, translational energies $E_i = \hbar^2 k_i^2/(2m)$ with $\hbar$ being the Planck constant, m is the particle mass, and k_i are the momentum eigenvalues that depend on the corresponding shape variable for each case that is considered, i.e., $k_i(l)$, $k_i(s)$, and $k_i(\theta)$, respectively, for the 1D domain with partition position l, the 2D domain with the inner disk position s, and the 2D domain with the inner square rotation angle θ. Let us assume a single particle for convenience since the functional behaviors of the statistical thermodynamic quantities would be exactly the same as the many-particle case because they are assumed to be noninteracting. For an N-particle analysis of the problem, see Ref. [42]. The thermal occupation probability of a level i is given by

$$p_i = \frac{1}{Z}\exp\left(-\frac{E_i}{k_BT}\right). \tag{11}$$

Then Helmholtz free energy, Gibbs entropy, and internal energy are written respectively as

$$F = -k_BT\ln Z, \tag{12a}$$

$$S = -k_B\sum_i p_i \ln p_i, \tag{12b}$$

$$U = \sum_i p_i E_i. \tag{12c}$$

In Fig. 6 we plot the functional behaviors of thermodynamic properties changing with the corresponding shape variables. Red, green, and blue curves respectively represent the thermodynamic properties of the 1D domain with moving partition, 2D nested domain with translating disk, and 2D nested domain with a rotating square. Partition function, free energy, entropy, and internal energy are represented by the colors from darker to lighter shades, respectively. In all cases, the partition function increases, as the total occupation probabilities increase. The reason for this can be understood via the following analysis. Classically, the partition function is a function of volume and temperature, as $Z \propto \mathcal{V}_n$ and $Z \propto T^{n/2}$. Therefore, classically one should not expect any variation in partition function under SIST, as the volume (as well as all other size parameters) stays constant. The changes in partition function can be understood by introducing the effective volume concept of the quantum boundary layer approach [42,43]. Although the apparent volume $\mathcal{V}$ of the object

remains unchanged, the effective volume $\mathcal{V}_{\text{eff}}$, which depends on the corresponding shape variable, changes. More information about the effective volume and quantum boundary layer concepts can be found in the Appendix. The effective volume is defined with additional terms including more complicated temperature dependencies. By definition, the effective volume is also directly proportional to the partition function and they share the same functional dependency. Hence, the partition function mimics the behavior of effective volume which is increased due to the emergent overlaps of quantum boundary layers [23]. Due to these overlaps, the domain becomes less confined locally (i.e., increase in local breadth). The partition function makes a slow start because the inner and outer boundaries are not close enough to each other for their quantum boundary layers to overlap (here we are not necessarily considering the zeroth order overlap, see for instance Fig. 10 in Ref. [23]). Once they are close enough, overlaps cause the effective volume to increase exponentially (due to the enhanced ground-state occupation), and hence the partition function as well, Fig. 6(a). However, after some point, the boundaries are so close to each other that effectively no particle can occupy the space in the squeezed part of the domain. Then moving the inner boundary becomes no different than extending the domain length as a whole (the particle cannot distinguish the inner boundary from the outer one as we also mentioned in Sec. IV). In such a case, the usual volume (length in 1D) dependence of the partition function is recovered and it increases linearly with l, Fig. 6(a).

These characteristic behaviors of the partition function are directly reflected in other thermodynamic properties as well, shown in Figs. 6(b)–6(d). Thermodynamic properties change negligibly at the region where the partition function does not change much. In the exponential increase region, free energy, entropy, and internal energy decrease together with the shape variable, which is a peculiar behavior having many counterintuitive consequences [23–25,46,71]. In the linear increase region, free energy and internal energy decrease, whereas entropy increases. This last behavior is ordinary as it is consistent with the expectations of classical thermodynamics. Characteristic functional behaviors of thermodynamic properties are quite similar in 1D and 2D translational SIST (compare to the red and green curves in Fig. 6). This is expected, since both operations are essentially the same (increasing the local breadth by squeezing the other parts of the domain) but just realized in different dimensions for different shapes. In the 2D rotational SIST, on the other hand, we see more of a sigmoidlike increase in the partition function. This leads to the simultaneous decrease of free energy, entropy, and internal energy with the shape variables in their full ranges. Monotonic decreases in free energy and internal energy are expected since the domain is effectively expanding under the rotational SIST, which is evident from the behavior of the partition function. This leads to a decrease in confinement energy which reduces the internal energy and effective expansion of the particles with increased $\mathcal{V}_{\text{eff}}$ is accompanied by the decrease in free energy. Such thermodynamic behaviors have been shown to be important to precisely calculate the heat and work exchanges in quantum Szilard engines [71].

The most interesting one of the shape-dependent thermodynamic behaviors is the spontaneous and simultaneous

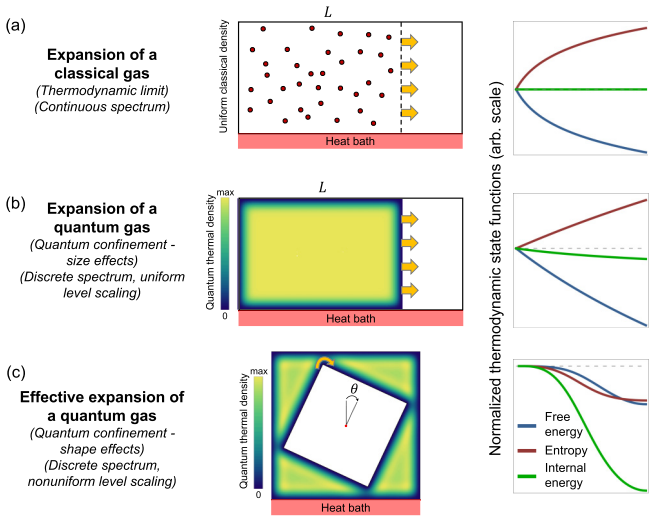

FIG. 7. Comparison of the isothermal expansions of unconfined (a) and confined gases with uniform (b) and nonuniform (c) level scalings. Blue, red, and green curves represent the variations of free energy, entropy, and internal energy, respectively, with the corresponding expansion parameters. Thermodynamic-state functions are normalized to their initial values and given in arbitrary scale since we only emphasize their functional behaviors here.

decrease of free energy and entropy under an isothermal, quasistatic SIST process [23]. A decrease in entropy is much more difficult to understand solely from the effective volume perspective. To understand the peculiarity of such a decrease, consider an isothermal expansion process. During the isothermal expansion of a classical ideal gas, free energy decreases, entropy increases, and internal energy stays constant, see Fig. 7(a). In the presence of quantum confinement, similar behaviors are observed except internal energy does not remain constant but decreases, Fig. 7(b), due to the confinement energy coming from the quantum size effects [7,72]. On the other hand, when a quantum confined gas effectively expands under SIST via a shape variable, free energy, entropy, and internal energy can spontaneously and simultaneously decrease [23], see Fig. 7(c). This counterintuitive behavior leads to some classically unexpected thermodynamic phenomena such as spontaneous transitions into lower entropy states, temperature-dependent work, isotropic heat and work exchanges, cooling by adiabatic compression or heating by adiabatic expansion, and work extraction occurring at the cold side (as opposed to hot side) of the cycles [23,46]. All of these extraordinary behaviors originate from the peculiar spectral changes due to SIST under quantum confinement at thermal equilibrium. Previously, these behaviors have been examined from a more physical perspective such as the variation of quantum boundary layers due to temperature in confined domains [23,46]. From the thermodynamics perspective, in-phase behavior of internal energy, free energy, and entropy causes many of these mentioned behaviors. Here we go even further and understand the fundamental underlying reason for these unconventional behaviors by directly examining the characteristic changes in the energy spectrum as well as their effects on the thermal probabilities and properties.

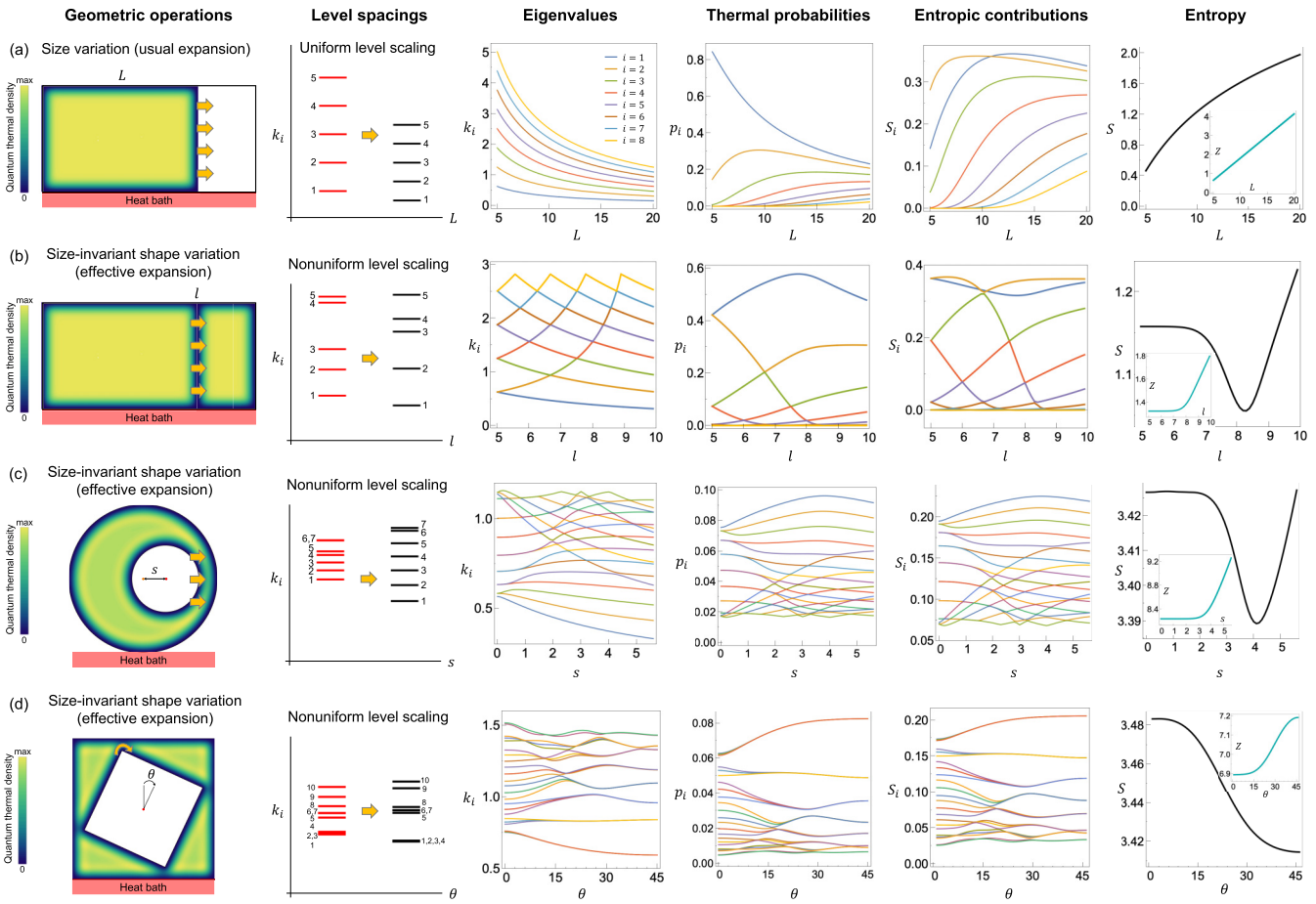

FIG. 8. Spectral and thermal signatures of entropy anomalies and consequences of nonuniform level scaling. The rows show the systems that are considered. Geometric operations and quantum thermal densities are shown for each system. Due to quantum confinement, density distributions are nonuniform even at thermal equilibrium. (a) Isothermal expansion of a quantum gas. The volume (length in 1D) of the gas increases as a whole. (b) Isothermal variation of the inner boundary (partition) of a box with a quantum gas. The actual volume stays constant, whereas the effective volume of the gas increases. (c) Isothermal variation of the inner boundary in the nested disk domain. (d) Isothermal variation of the inner boundary in the nested square domain. Columns in each row represent respectively the system, scaling of energy levels, variation of first few eigenvalues with respect to the corresponding size or shape variable, variation of thermal occupation probabilities of each state i, and variation in the contributions of each state i to the entropy and finally the total entropy of the system. Inset figures show the changes in the partition functions (corresponding to the expansion or effective expansions).

VIII. QUANTUM THERMAL AVALANCHE

Even though the effective volume and quantum boundary layer concepts provide useful physical insights on how these types of unconventional changes occur in systems under SIST, by analyzing the eigenspectra, we can understand more about the nature of these changes as well as their physical origins. We examine the origins of the entropy anomalies in Fig. 8 in the eigenspectra and thermal probabilities. Columns represent the isothermal geometric operations in the considered systems, corresponding level spacings, behavior of the first few momentum eigenvalues, thermal probabilities, contributions of each state to the entropy, and, finally, the variation of the entropy of the system with respect to the corresponding geometric control variable.

Increasing the length of a box uniformly decreases the eigenvalues, resulting in a continuous decrease in the ground-state occupation probability and successive increments in the excited-state occupations, Fig. 8(a). As a result, entropy monotonically increases with the increasing length. Under SIST, however, changing the position of the partition causes a nonuniform change in the eigenvalues so that some eigenvalues rise while others descend and even undulate (going back and forth in a zigzag movement), Fig. 8(b). As a result of these nonuniform changes, in certain parameter ranges the ground-state occupation probability increases, while the thermal occupation probabilities of excited states exhibit undulating behaviors. Due to the increased occupation of the ground state as well as the accumulative behavior of undulating occupation probabilities of excited states, entropy decreases in the peculiar region despite the increase in effective volume; see the inset figures in the entropy subfigure. The winner of the competition between these two competing mechanisms essentially depends on the specific geometric configuration of the system. Similar behaviors are also observed for other SISTs having nonuniform level scalings such as the translational 2D [Fig. 8(c)] and rotational 2D [Fig. 8(d)] ones. Note that in all cases the geometric operations cause

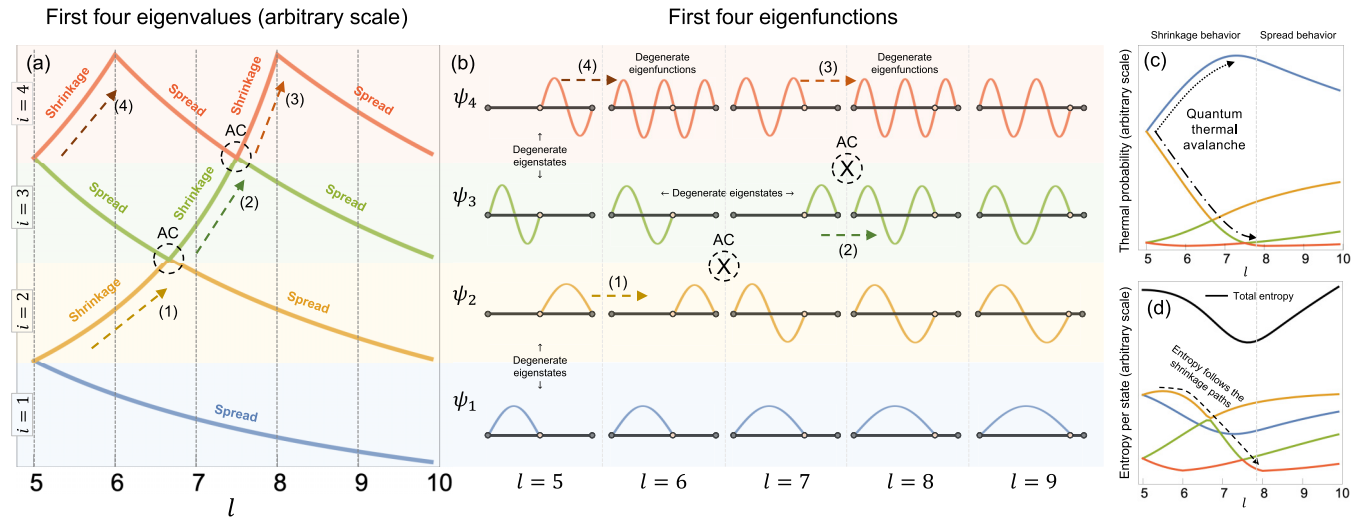

FIG. 9. Rush to the ground state: quantum thermal avalanche. (a) Behaviors of the first four eigenvalues with the inner boundary (partition) position l in a 1D particle in a box. Partition is at the center for $l = 5$ and at the right boundary of the box for $l = 10$. (b) Behaviors of the first four eigenfunctions. Nonuniform level scaling is apparent from the mixed behaviors of spread and shrinkage of the eigenfunctions. Geometry-induced avoided crossings (AC) are observed due to eigenstate swapping. (c) Thermal occupation probabilities of the first four states. Shrinkages of the excited-state eigenfunctions cause swapping between the ground-state and excited-state occupations leading to an abrupt increase in the ground-state occupation probability, which we call quantum thermal avalanche. (d) The entropy contributions of the first four states and the entropy are shown with colored and black curves, respectively.

some sort of expansion, as is evident from the increase in the number of available states characterized by the increase in the partition functions shown in the insets of the entropy subfigures of Fig. 8.

Let us focus on the simplest one of the considered systems to understand spontaneous entropy reduction. Consider the 1D particle in a box with a moving partition (1D translational SIST) that is confined enough (e.g., the temperature is low or size is small enough) to be represented by the thermal probabilities of just the first four eigenvalues (for simplicity). In Fig. 9(a), we plot the variation of the first four eigenvalues k_i with the shape variable l, the position of the partition. In Fig. 9(b), we plot the variations of the corresponding eigenfunctions, ψ_i. We present the thermal probabilities p_i in Fig. 9(c) and contributions to the entropy of each state S_i in Fig. 9(d). Entropy is the sum of the contributions of all four states, which is shown with the black curve. At $l = 5$, the partition starts at the center and the ground state is degenerate, occupying both left and right compartments. With the movement of the partition to the right, the ground state of the system ($i = 1$) monotonically decreases with the increasing length of the left compartment where it sits, see ψ_1 in the blue row of Fig. 9(b). However, when we look at the behavior of the first excited state ($i = 2$), we see an undulating (zigzag) behavior as a manifestation of nonuniform level scaling. It initially increases and then at some point reverses its behavior and decreases just like the ground state does. As it is seen from the yellow row of Fig. 9(b), the first excited-state eigenfunction squeezes into the smaller part of the domain between $l = 5$ and $l = 6$ constituting the ground state of the right compartment. However, at a point between $l = 6$ and $l = 7$, occupying the first excited state of the larger compartment becomes energetically more favorable than occupying the ground state of the smaller compartment and it switches into the left compartment where its wavelength can stay larger. In other words, ψ_2 first shrinks as the right compartment's ground state then transfer itself to the left compartment's first excited state and spread there with the right-moving partition. Similar shrinkage and spread behaviors of the eigenfunctions are seen in the higher eigenstates. Eigenstate swappings manifest themselves as geometry-induced avoided crossings in the eigenspectrum. Note that these are different than the usual avoided crossing phenomenon because in our case this behavior occurs due to the geometry of the system rather than interactions between the states. Additionally, due to the idealistic nature of the chosen system, the crossings are infinitesimally avoided (still they do not cross each other). The avoided crossings are gaped in other less idealistic systems, see Figs. 8(c) and 8(d).

Unlike in the usual size variation, in this case, expansion and contraction occur simultaneously in the different parts of the system. Shrinkage and spread behaviors of eigenfunctions directly determine the faith of the entropy under SISTs. Peculiarities in entropy arise from the shrinkage behaviors of the eigenfunctions, marked by the colored-dashed arrows. While the spreading of the eigenfunction along with the corresponding monotonic decrease of the eigenvalues is a common behavior due to the physics of the expansion, the shrinkage of some eigenfunctions in fact results in the increase of the corresponding eigenvalues. These changes in the spectra manifest themselves as opposite behaviors in the thermal occupation probabilities, Fig. 9(c). Because of the shrinkages thermal occupation probability of the ground state abruptly increases while that of the first excited state decreases and higher excited states show undulating behavior, see Fig. 9(c). This is a completely opposite behavior of an expanding system. We call this effect quantum thermal avalanche, due to the excessive occupation of the ground state occurring in quantum-confined

systems at the thermal equilibrium. The rationale behind the name "avalanche" lies in the fact that Helmholtz free energy decreases during the phenomenon, defining the spontaneous transition towards lower entropy states once initiated. Although the system is effectively expanding with moving partition, entropy decreases because of the sharp increase in the ground-state occupation probability which makes the system less disordered. While there are more available states (as the partition function increases), most of them sit in the ground state not contributing to the entropy. This explains why the entropy decreases between $l = 5$ and $l = 8$. It basically follows the shrinkages of the eigenfunctions, see the dashed black arrows in Figs. 9(c) and 9(d) and compare them with the dashed colored arrows denoting the shrinkages. Notice how smoothly they represent the different behaviors with eigenstate swaps at the avoided crossings. On the other hand, between $l = 8$ and $l = 10$, all four eigenfunctions coherently spread out with the moving partition. This causes the recovery of the usual expansion behavior of the system in the thermal probabilities so that ground-state occupation decreases and excited-state occupations increase successively, Fig. 9(c). Hence, entropy increases between $l = 8$ and $l = 10$, Fig. 9(d).

Quantum thermal avalanche is a direct result of the nonuniform level scaling that is caused by the geometric level couplings due to SISTs. Despite the shrinkages and spreads occurring simultaneously in the system (since one compartment gets smaller as the other gets larger), the shrinkage behaviors could dominate the overall behavior for the wide range of the control variable. In other words, the decrease in entropy due to the contraction of the smaller compartment dominates the increase in entropy due to the expansion of the larger compartment. As we mentioned earlier, this asymmetricity comes from the decay of occupation probabilities in the smaller part. The quantum thermal avalanche concept also explains the exponential increase of the partition function between $l = 5$ and $l = 8$, which is basically due to the enhanced ground-state occupation.

Similarly to entropy, changes in free energy and internal energy can also be interpreted from the perspective of ground-state reduction and quantum thermal avalanche. Internal energy is basically a sum over the energy levels times the corresponding thermal occupation probabilities. Free energy can also be written by factoring out the ground state and defining excited states over the level differences, which brings out the explicit ground-state dependence as a separate term. Due to these explicit dependencies on the ground state, a decrease of the first eigenvalue directly leads to the reduction of internal energy and free energy. The changes in their slopes in Fig. 6 directly come from the changing behavior of the ground-state occupation probability shown in Fig. 9(c). The maximum of the ground-state thermal occupation probability separates the region that is dominated by the shrinkages (quantum thermal avalanche) and the spreads (the usual expansion behavior). All of our explanations are valid for other types of SISTs as our interpretations can be applied to the subfigures shown in Figs. 8(c) and 8(d).

While all of these are inherently boundary effects, they are not seen in classical systems because energy quantization only becomes appreciable in quantum-confined systems. The quantum thermal avalanche effect and all the other consequences of the SIST rely on the importance of the ground and low-lying states in determining the physical properties of the system. Otherwise, for larger (unconfined) systems with highly occupied states, these effects will be negligible, as we have shown in Fig. 3, since the spectral differences become indistinguishable. For weakly confined or unconfined and classical systems, SISTs do not cause any change in the thermodynamic properties of the particles since their wave nature is not strong enough to feel the boundary modifications as they act almost like point particles. In classical systems, thermal occupation of higher and higher levels will dominate over these ground-state and low-lying eigenstate behaviors, and hence the quantum thermal avalanche effect disappears.

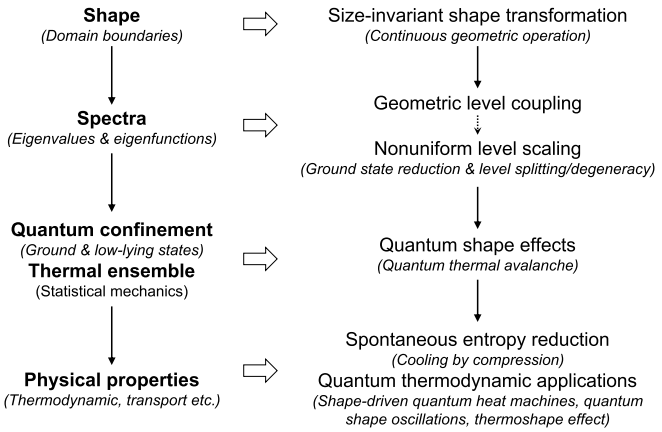

FIG. 10. Summary and physical consequences of the spectral signatures of size-invariant shape transformation.

IX. CONCLUSION

In this paper, we investigated the characteristic modifications in the Dirichlet spectra of various domains due to the boundary effects under a specific geometric transformation called SIST. There are two types of SIST: translational and rotational. Both cause similar counterintuitive thermodynamic behaviors. For convenience, we worked with 1D and 2D systems but our results hold in any dimension. In fact, the three cases that we considered are quite general and comprehensive. By using the procedures of SIST, one can design arbitrary domains in any dimension exhibiting similar behaviors. Our work emphasizes, perhaps once again, how subtle effects can appear when two boundaries come very close to each other at nanoscale systems.

We gave the general outline of our work in Fig. 10. The shape of a domain determines its spectra. A continuous geometric operation of SIST creates a particular geometric coupling between the levels, which gives rise to a nonuniform scaling of levels. Quantum confinement leads to an increase in the importance of the ground state in determining the physical properties of the system. Hence, the ground-state reduction and spectral gaps cause some behaviors that are not observed in classical systems, such as quantum thermal avalanche under the umbrella of quantum shape effects. As a result of these, peculiar behaviors are seen in thermodynamic properties such as the spontaneous transition into the lower entropy states.

Quantum shape effects have many novel quantum thermodynamic applications, such as shape-driven quantum heat machines [23,46], quantum shape oscillations in thermodynamic properties of Fermionic systems [25], and thermoshape effect for energy harvesting with nanostructures [24].

Designing nanostructures with almost arbitrary sizes and shapes is possible with the state-of-the-art nanotechnology [73–75]. SISTs are therefore within the reach of existing experimental setups and utilizing the peculiar quantum thermodynamic features of SISTs could be considered as a viable direction for nanoscience and nanoenergy technologies. Our work could provide a theoretical basis for designing confinement geometries that could enhance the performance and efficiency of quantum thermal machines. Apart from nanostructures, our spectral findings could also be applied to the studies of quantum billiards, graphs as well as optical cavities. In fact, our work could basically have implications for all types of few-level systems. Beyond the spectral geometry, the ideas and findings we presented here could also provide new insights to the spectral theory in a broader sense.

APPENDIX: TEMPERATURE-DEPENDENT EFFECTIVE VOLUME AND QUANTUM BOUNDARY LAYER

We used a concept called effective volume to explain some of the thermodynamic behaviors. Here we give brief information about the effective volume and quantum boundary layer concepts. More detailed examinations can be found in Section 2.3 of Ref. [46]. A single quantum particle occupies the confined space in an inhomogeneous way even at thermal equilibrium due to its wave nature [43]. Thermally weighted quantum probability density (quantum thermal density in short) of the confined particle is given by

$$n(T,\mathbf{r}) = \sum_i p_i(T)|\psi_i(\mathbf{r})|^2, \tag{A1}$$

where $\mathbf{r}$ is the position vector and ψ_i is the eigenfunction of the ith state. Equation (A.1) contains both the thermal and quantum probabilities, effectively capturing the quantum-thermodynamic nature of the confined system. We used this equation to plot the quantum thermal densities in Figs. 7 and 8.

As a result of the nonuniform density distribution even at thermal equilibrium, effectively empty regions form near the domain boundaries, which is called the quantum boundary layer [43–45]. The thickness of the quantum boundary layer for a confined ideal gas obeying Maxwell-Boltzmann distribution is universal (shape-independent) and exactly one-fourth of the thermal de Broglie wavelength,

$$\delta(T) = \frac{\lambda_{\rm th}(T)}{4}, \tag{A2}$$

where $\lambda_{\rm th} = \hbar\sqrt{2\pi}/\sqrt{mk_BT}$ is the thermal de Broglie wavelength of particles.

Since the confined particles effectively occupy the rest of the domain that is not excluded by quantum boundary layers, one can introduce a new, effective volume by removing the quantum boundary layers from the actual volume. In the case of SISTs, quantum boundary layers can overlap, which increases the available domain for particles to occupy [23]. Thereby the effective volume is written as

$$\mathcal{V}_{\rm eff}(T,\gamma) = \mathcal{V} - \mathcal{V}_{\rm qbl}(T) + \mathcal{V}_{\rm ovr}(T,\gamma), \tag{A3}$$

where γ is a generic shape variable. It has been shown that effective volume can accurately predict both quantum size and quantum shape effects [23,42]. An interesting feature of the effective volume is its temperature dependence manifested in the thermal de Broglie wavelength. As a result, pressure or torque due to quantum confinement effects depends on temperature. This makes the work term in the first law of thermodynamics temperature dependent, giving rise to some classically impossible thermodynamic cycles as they are investigated in Refs. [23,46].

[1] H. Urakawa, *Spectral Geometry of the Laplacian: Spectral Analysis and Differential Geometry of the Laplacian* (World Scientific, Singapore, 2017).

[2] H. P. Baltes and E. R. Hilf, *Spectra of Finite Systems* (Bibliographisches Institut, Gotha, 1976).

[3] R. K. Pathria, An ideal quantum gas in a finite-sized container, Am. J. Phys. **66**, 1080 (1998).

[4] N. Z. Vagidov V. V. Mitin, and D. I. Sementsov, *Quantum Mechanics for Nanostructures* (Cambridge University Press, Cambridge, UK, 2010).

[5] C. W. J. Beenakker and H. van Houten, Quantum transport in semiconductor nanostructures, Solid State Phys. **44**, 1 (1991).

[6] A. D. Yoffe, Low-dimensional systems: Quantum size effects and electronic properties of semiconductor microcrystallites (zero-dimensional systems) and some quasi-two-dimensional systems, Adv. Phys. **51**, 799 (2002).

[7] A. Sisman and I. Müller, The casimir-like size effects in ideal gases, Phys. Lett. A **320**, 360 (2004).

[8] Y. A. Koksharov, Magnetism of nanoparticles: Effects of size, shape, and interactions, in *Magnetic Nanoparticles*, edited by S. P. Gubin (Wiley-VCH, Hoboken, NJ, 2009), Chap. 6, pp. 197–254.

[9] A. J. McNamara, B. J. Lee, and Z. M. Zhang, Quantum size effect on the lattice specific heat of nanostructures, Nanoscale Microscale Thermophys. Eng. **14**, 1 (2010).

[10] E. Roduner, *Nanoscopic Materials, Size-Dependent Phenomena* (RSC Publishing, Cambridge, UK, 2006).

[11] Ren Sh. Y, *Electronic States in Crystals of Finite Size: Quantum Confinement of Bloch Waves* (Springer, Singapore, 2005).

[12] T. Fülöp and I. Tsutsui, Boundary effect of a partition in a quantum well, J. Phys. A: Math. Theor. **40**, 4585 (2007).

[13] *Size Effects in Nanostructures: Basics and Applications*, edited by L. Miu and V. Kuncser, Springer Series in Materials Science Vol. 205 (Springer, Berlin, 2014).

[14] H. T. Quan, P. Zhang, and C. P. Sun, Quantum heat engine with multilevel quantum systems, Phys. Rev. E **72**, 056110 (2005).

[15] H. T. Quan, Y.-X. Liu, C. P. Sun, and F. Nori, Quantum thermodynamic cycles and quantum heat engines, Phys. Rev. E **76**, 031105 (2007).

[16] M. Campisi and R. Fazio, The power of a critical heat engine, Nat. Commun. **7**, 11895 (2016).

[17] D. Gelbwaser-Klimovsky, A. Bylinskii, D. Gangloff, R. Islam, A. Aspuru-Guzik, and V. Vuletic, Single-Atom Heat Machines Enabled by Energy Quantization, Phys. Rev. Lett. **120**, 170601 (2018).

[18] A. Levy and D. Gelbwaser-Klimovsky, in *Quantum Features and Signatures of Quantum Thermal Machines* (Springer International Publishing, Cham, 2018), pp. 87–126.

[19] G. Thomas, D. Das, and S. Ghosh, Quantum heat engine based on level degeneracy, Phys. Rev. E **100**, 012123 (2019).

[20] S. Chatterjee, A. Koner, S. Chatterjee, and C. Kumar, Temperature-dependent maximization of work and efficiency in a degeneracy-assisted quantum stirling heat engine, Phys. Rev. E **103**, 062109 (2021).

[21] L. Chen, Z. Meng, Y. Ge, and F. Wu, Performance analysis and optimization for irreversible combined carnot heat engine working with ideal quantum gases, Entropy **23**, 536 (2021).

[22] J. L. D. de Oliveira, M. Rojas, and C. Filgueiras, Two coupled double quantum-dot systems as a working substance for heat machines, Phys. Rev. E **104**, 014149 (2021).

[23] A. Aydin and A. Sisman, Quantum shape effects and novel thermodynamic behaviors at nanoscale, Phys. Lett. A **383**, 655 (2019).

[24] A. Sisman, A. Aydin, and J. Fransson, Thermoshape effect for energy harvesting with nanostructures, J. Phys. D: Appl. Phys. **53**, 375501 (2020).

[25] A. Aydin, J. Fransson, and A. Sisman, Quantum shape oscillations in the thermodynamic properties of confined electrons in core–shell nanostructures, J. Phys.: Condens. Matter **34**, 025301 (2022).

[26] M. Kac, Can one hear the shape of a drum? Am. Math. Mon. **73**, 1 (1966).

[27] L. N. Trefethen and Timo Betcke, Computed eigenmodes of planar regions, in *Contemporary Mathematics* (American Mathematical Society, Providence, RI, 2006), pp. 297–314.

[28] O. Giraud and K. Thas, Hearing shapes of drums: Mathematical and physical aspects of isospectrality, Rev. Mod. Phys. **82**, 2213 (2010).

[29] W.-S. Dai and M. Xie, The number of eigenstates: Counting function and heat kernel, J. High Energy Phys. 02 (2009) 033.

[30] P. Exner and P. Seba, Bound states in curved quantum waveguides, J. Math. Phys. **30**, 2574 (1989).

[31] D. Kouznetsov and J. V. Moloney, Boundary behaviour of modes of a dirichlet laplacian, J. Mod. Opt. **51**, 1955 (2004).

[32] D. N. Maksimov and A. F. Sadreev, Bound states in elastic waveguides, Phys. Rev. E **74**, 016201 (2006).

[33] G. F. Dell'Antonio and E. Costa, Effective schrodinger dynamics on ϵ-thin dirichlet waveguides via quantum graphs: I. star-shaped graphs, J. Phys. A: Math. Theor. **43**, 474014 (2010).

[34] A. L. Delitsyn, B. T. Nguyen, and D. S. Grebenkov, Trapped modes in finite quantum waveguides, Eur. Phys. J. B **85**, 176 (2012).

[35] E. B. Kolomeisky, H. Zaidi, L. Langsjoen, and J. P. Straley, Weyl problem and casimir effects in spherical shell geometry, Phys. Rev. A **87**, 042519 (2013).

[36] E. J. Heller, Bound-State Eigenfunctions of Classically Chaotic Hamiltonian Systems: Scars of Periodic Orbits, Phys. Rev. Lett. **53**, 1515 (1984).

[37] S. Åberg, T. Guhr, M. Miski-Oglu, and A. Richter, Superscars in Billiards: A Model for Doorway States in Quantum Spectra, Phys. Rev. Lett. **100**, 204101 (2008).

[38] P. Yu, B. Dietz, H.-Y. Xu, L. Ying, L. Huang, and Y.-C. Lai, Kac's Isospectrality Question Revisited in Neutrino Billiards, Phys. Rev. E **101**, 032215 (2020).

[39] M. F. Crommie, C. P. Lutz, and D. M. Eigler, Confinement of electrons to quantum corrals on a metal surface, Science **262**, 218 (1993).

[40] D. P. Murdock J. T. Londergan and J. P. Carini, *Binding and Scattering in Two-dimensional Systems: Applications to Quantum Wires, Waveguides, and Photonic Crystals*, 1st ed., Lecture Notes in Physics Monographs (Springer, Berlin, 2000).

[41] H.-D. Li, S.-L. Li, Y.-J. Chen, W.-D. Li, and W.-S. Dai, Energy spectrum of interacting gas: Cluster expansion method, Chem. Phys. **559**, 111537 (2022).

[42] A. Aydin and A. Sisman, Origin of quantum shape effect, arXiv:2301.12551.

[43] A. Sisman, Z. F. Ozturk, and C. Firat, Quantum boundary layer: A non-uniform density distribution of an ideal gas in thermodynamic equilibrium, Phys. Lett. A **362**, 16 (2007).

[44] C. Firat and A. Sisman, Universality of the quantum boundary layer for a maxwellian gas, Phys. Scr. **79**, 065002 (2009).

[45] C. Firat, A. Sisman, and Z. F. Ozturk, Thermodynamics of gases in nano cavities, Energy **35**, 814 (2010).

[46] A. Aydin, Quantum Shape Effects, Ph.D. thesis, Energy Institute, Istanbul Technical University, Istanbul (2020).

[47] H. Weyl, Über die asymptotische verteilung der eigenwerte, Nachr. Ges. Wiss. Goettingen, Math. Phys. Kl. **1911**, 110 (1911).

[48] I. Bowser, K. Kiers, E. Mitchell, and J. Kiers, Weyl's problem: A computational approach, Am. J. Phys. **88**, 769 (2020).

[49] A. Aydin and A. Sisman, Discrete density of states, Phys. Lett. A **380**, 1236 (2016).

[50] A. Aydin, T. Oikonomou, G. B. Bagci, and A. Sisman, Discrete and weyl density of states for photonic dispersion relation, Phys. Scr. **94**, 105001 (2019).

[51] R. D. Benguria, H. Linde, and B. Loewe, Isoperimetric inequalities for eigenvalues of the laplacian and the schrödinger operator, Bull. Math. Sci. **2**, 1 (2012).

[52] J. R. Kuttler and V. G. Sigillito, Eigenvalues of the laplacian in two dimensions, SIAM Rev. **26**, 163 (1984).

[53] M. A. Khabou, L. Hermi, and M. B. H. Rhouma, Shape recognition using eigenvalues of the dirichlet laplacian, Pattern Recogn. **40**, 141 (2007).

[54] "breadth," Retrieved December 7, 2022, from https://www.dictionary.com/browse/breadth.

[55] Y. S. E. Brian Davies, *Spectral Theory and Geometry*, 1st, ed., London Mathematical Society Lecture Note Series (Cambridge University Press, Cambridge, UK, 1999).

[56] A. Henrot, *Shape Optimization and Spectral Theory*, 1st ed. (Sciendo, Warsaw, 2017).

[57] A. Henrot, in *Isoperimetric Inequalities for Eigenvalues of the Laplacian* (Springer International, Cham, 2018), pp. 47–88.

[58] S. Loncaric, A survey of shape analysis techniques, Pattern Recogn. **31**, 983 (1998).
[59] J. Zheng, Q. Sun, H. Zheng, D. Wei, Z. Li, and L. Gao, Three-dimensional particle shape characterizations from half particle geometries, Powder Technol. **367**, 122 (2020).
[60] H. Wadell, Sphericity and roundness of rock particles, J. Geol. **41**, 310 (1933).
[61] R. J. B. Wets and R. Tyrrell Rockafellar, *Variational Analysis*, 1st ed. Grundlehren der mathematischen Wissenschaften No. 317 (Springer, Berlin, 1998).
[62] M. van Kreveld, T. Miltzow, T. Ophelders, W. Sonke, and J. L. Vermeulen, Between shapes, using the hausdorff distance, Comput. Geom. **100**, 101817 (2022).
[63] R. Basri, L. Costa, D. Geiger, and D. Jacobs, Determining the similarity of deformable shapes, Vis. Res. **38**, 2365 (1998).
[64] R. C. Veltkamp and M. Hagedoorn, Shape similarity measures, properties and constructions, in *Advances in Visual Information Systems*, edited by R. Laurini (Springer, Berlin, 2000), pp. 467–476.
[65] V. A. Zalgaller and Y. D. Burago, *Geometric Inequalities*, 1st ed., Grundlehren der mathematischen Wissenschaften No. 285 (Springer, Berlin, 1988).
[66] H.-J. Stockmann, *Quantum Chaos: An Introduction* (Cambridge University Press, Cambridge, UK 1999).
[67] D. Gelbwaser-Klimovsky, W. Kopylov, and G. Schaller, Cooperative efficiency boost for quantum heat engines, Phys. Rev. A **99**, 022129 (2019).
[68] T. R. de Oliveira and D. Jonathan, Efficiency gain and bidirectional operation of quantum engines with decoupled internal levels, Phys. Rev. E **104**, 044133 (2021).
[69] W. S. Dai and M. Xie, Quantum statistics of ideal gases in confined space, Phys. Lett. A **311**, 340 (2003).
[70] W.-S. Dai and M. Xie, Geometry effects in confined space, Phys. Rev. E **70**, 016103 (2004).
[71] A. Aydin, A. Sisman, and R. Kosloff, Landauer's principle in a quantum szilard engine without maxwell's demon, Entropy **22**, 294 (2020).
[72] A. Aydin and A. Sisman, Discrete nature of thermodynamics in confined ideal fermi gases, Phys. Lett. A **378**, 2001 (2014).
[73] M. Tajik, B. Rauer, T. Schweigler, F. Cataldini, J. Sabino, F. S. Møller, S.-C. Ji, I. E. Mazets, and J. Schmiedmayer, Designing arbitrary one-dimensional potentials on an atom chip, Opt. Express **27**, 33474 (2019).
[74] N. Navon, R. P. Smith, and Z. Hadzibabic, Quantum gases in optical boxes, Nat. Phys. **17**, 1334 (2021).
[75] E. Busley, L. E. Miranda, A. Redmann, C. Kurtscheid, K. K. Umesh, F. Vewinger, M. Weitz, and J. Schmitt, Compressibility and the equation of state of an optical quantum gas in a box, Science **375**, 1403 (2022).